A supervoxel-based segmentation method for prostate MR images

Zhiqiang Tian[1], LiZhi Liu[1], Baowei Fei [1,2*]

[1]Department of Radiology and Imaging Sciences, Emory University, Atlanta, GA
[2]Department of Biomedical Engineering, Emory University and Georgia Institute of Technology
*Corresponding author: bfei@emory.edu; Website: http://feilab.org

ABSTRACT

Accurate segmentation of the prostate has many applications in prostate cancer diagnosis and therapy. In this paper, we propose a "Supervoxel" based method for prostate segmentation. The prostate segmentation problem is considered as assigning a label to each supervoxel. An energy function with data and smoothness terms is used to model the labeling process. The data term estimates the likelihood of a supervoxel belongs to the prostate according to a shape feature. The geometric relationship between two neighboring supervoxels is used to construct a smoothness term. A three-dimensional (3D) graph cut method is used to minimize the energy function in order to segment the prostate. A 3D level set is then used to get a smooth surface based on the output of the graph cut. The performance of the proposed segmentation algorithm was evaluated with respect to the manual segmentation ground truth. The experimental results on 12 prostate volumes showed that the proposed algorithm yields a mean Dice similarity coefficient of 86.9%±3.2%. The segmentation method can be used not only for the prostate but also for other organs.

Keywords: Magnetic resonance imaging (MRI), prostate cancer, segmentation, supervoxel, 3D graph cut, 3D level set

1. INTRODUCTION

It is estimated that there are 233,000 new cases of prostate cancer and 29,480 deaths from prostate cancer in the USA in 2014 [1]. Magnetic resonance imaging (MRI) has been increasingly used for the detection and diagnosis of prostate cancer [2-8]. Prostate delineation on MRI images helps physicians to measure the prostate size and help for treatment planning. However, prostate segmentation is a non-trivial because of the similar MR intensities between the prostate and adjacent tissue and because of the MR intensity inhomogeneity in the prostate region. Moreover, the prostate has a wide variety of shape appearance among different patients.

There are extensive studies [3, 9-14] in delineating the prostate surface from MRI. Qiu et al. [3] proposed a global optimization-based approach to segment T2 weighted MRI by enforcing the geometrically axial symmetry of the prostate shapes. This method coherently segmented a series of 2-D slices. Toth [9] presented a novel multi-feature landmark-free active appearance model for segmenting 2-D medical images. These methods yield good results but cannot handle medical images in a 3D manner. Egger [12] proposed an automated segmentation algorithm by applying a 3D graph-based algorithm for prostate segmentation. This method had a high computational cost due to their pixel-based manner. To resolve these problems, we propose a supervoxel-based 3D graph cuts method for segmenting the prostate.

We cluster groups of similar pixels into supervoxels, which are used to compute robust local statistics. This supervoxel-based method reduces the computational and memory costs without sacrificing accuracy because supervoxels naturally respect the object surface. The output of the graph cuts is used as an initialization for 3D level set based segmentation [15, 16], which can produce smooth prostate surfaces.

2. METHODS

An overview of the proposed method is shown in Fig. 1. Given a 3D MR volume, supervoxels are first generated by an efficient algorithm as described below. This is the key step for the proposed method. Supervoxel is the basic processing unit of our method, which reduces the computational and memory cost significantly. Secondly, the initial segmentation is obtained by minimizing the supervoxel-based energy function using a 3D graph cut algorithm. Finally, a 3D level set algorithm is adopted to smooth the prostate surface of the initial segmentation. The initial segmentation is close to the true surface, so it makes the level set converge quickly.
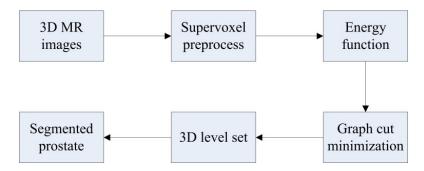

Figure 1. The framework of the proposed method.

2.1 Supervoxel

We consider one MR slice as a 2D image. "Superpixel" is a set of adjacent pixels in a slice with similar intensity or/and texture, while "Supervoxel" is a set of superpixels with similar intensity in the 3D volume. Fig. 2 demonstrates the supervoxels and their geometric relationships.
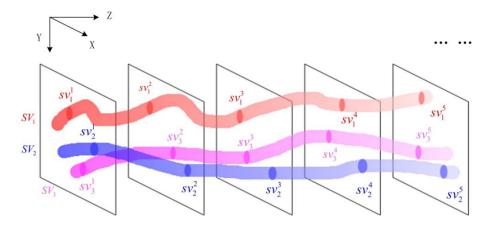

Figure 2. Supervoxels and their geometric relations in the 3D medical image volume.

An intersection between a supervoxel SV_i and Slice j is a superpixel sv_i^j. Supervoxel is defined as:

$$SV_i = \{sv_i^j, j = 1, \dots, |SV_i|\}, i = 1, \dots, M \tag{1}$$

where M is the number of the supervoxels in an MRI volume, $|SV_i|$ is the lifespan of the superpvoxel SV_i. The j-th superpixel of SV_i is sv_i^j, which consists of a set of pixels in one slice. Note that, different supervoxels may have different beginnings, endings, and different lifespans. In this work, supervoxels are obtained by using a simple linear iterative clustering method (SLIC) [17].

2.2 Energy function based on supervoxels

Graph cut [18] has been improved to be an efficient method [12] for segmenting 3D medical images. We consider prostate segmentation as a supervoxel labeling problem in a 3D graph. The superpvoxels are labeled as the prostate or background by optimizing an energy function. The energy function is defined as:

$$E(l) = \sum_{SV \in \Omega} D_{SV}(l_{SV}) + \gamma \sum_{\{SV_p, SV_q\} \in N} V_{SV_p, SV_q}(l_{SV_p}, l_{SV_q}) \tag{2}$$

where l is the label of the supervoxel, Label 1 represents the prostate, while Label 0 corresponds to the background, $N \in SV \times SV$ is a neighborhood. We assume that N contains a supervoxel pair $\{SV_p, SV_q\}$ which has a common boundary in one slice at least. The data term $D_{SV}(l_{SV})$ quantifies the distance of each supervoxel to a proposed shape model. The smoothness term $V_{SV_p, SV_q}(l_{SV_p}, l_{SV_q})$ quantifies how likely two supervoxels have the same label. The parameter γ balances the weight between the data term and the smoothness term.

In this work, a shape model is proposed to build the data term. Three key slices are selected as the initialization, which are selected from the apex, base, and middle of the prostate. Four to six points are marked for each key slice. Based on these initializations, two semi-ellipsoids are fitted. One is toward to the apex, the other is toward to the base. Note that these two fitted surfaces of semi-ellipsoids are not accurate. They are just used to compute the shape data term.

Once the fitted surfaces are obtained, the prostate and the background shape data term can be defined as:

$$D_{SV}(l_{SV} = 1) = -\log f(S_{SV}|l_{SV} = 1) \tag{3}$$
$$D_{SV}(l_{SV} = 0) = -\log f(S_{SV}|l_{SV} = 0) \tag{4}$$

where S_{sv} represents the mean value of shape feature of a supervoxel. f is defined as:

$$f(S_{SV}|l_{SV} = 1) = 1 - f(S_{SV}|l_{SV} = 0) = \frac{1}{1 + \exp(-\beta*(d-k))} \tag{5}$$

where d is the distance of a pixel to the fitted surfaces. k and β are shape feature parameters which control the fatness and slope of the shape.

The affinities of each pair of neighboring supervoxels SV_p and SV_q are used to compute the smoothness term. The supervoxels that are close to each other and have more common slices will be grouped together. Based on this principle, the smoothness term is defines as:

$$\sum_{\{SV_p, SV_q\} \in N} V_{SV_p, SV_q}(l_{SV_p}, l_{SV_q}) = |l_{SV_p} - l_{SV_q}| \frac{SV_p \cap SV_q}{\max(|SV_p|, |SV_q|)} \tag{6}$$

where $SV_p \cap SV_q$ stands for the number of common slices between two neighboring supervoxels. $|SV_p|$ and $|SV_q|$ are the number of slices (lifespan) of supervoxel SV_p and SV_q, respectively. This geometry based smoothness term encourages supervoxels that have similar locations and share more common slices to be assigned as the same label.

Once data term and smoothness term are obtained, the energy function can be minimized by the graph cut algorithm. Each supervoxel will be assigned a binary label. The pixels in the same supervoxel have the same label. Then the prostate surface can be derived from the labeled volume data.

2.3 3D level set

The supervoxel-based graph cut algorithm is an efficient method. However, the output may be not satisfactory when the supervoxel fails to find the boundary of the prostate accurately. To solve this problem, the prostate surface obtained from the graph cut should be refined. 3D level set is adopted in our method to refine the prostate surface. As the surface is good enough for the initialization of the level set algorithm, only several iterations are needed to achieve convergence.

2.4 Evaluation metrics

Four evaluation metrics are used to evaluate the performance, which are DICE similarity coefficient (DSC), relative volume difference (RVD), Hausdorff distance (HD), and average surface distance (ASD) [3, 19]. The DSC is calculated by:

$$DSC = \frac{2|V_{gt} \cap V_{alg}|}{|V_{gt}| + |V_{alg}|} \tag{7}$$

where $|V_{gt}|$ is the number of voxels in the segmentation of the ground truth and $|V_{alg}|$ is the number of voxels in the segmentation of the proposed algorithm. The RVD is computed as:

$$RVD = 100 \times \left(\frac{|V_{gt}|}{|V_{alg}|} - 1\right) \tag{8}$$

The RVD is used to evaluate whether the algorithm tends to over-segment or under-segment the prostate. To compute the HD and ASD, a distance from a voxel x to a surface Y is defined firstly as $d(x, Y) = \min_{y \in Y} \|x - y\|$.

The HD between two surfaces X and Y is calculated by:

$$HD(X, Y) = \max\left[\max_{x \in X} d(x, Y), \max_{y \in Y} d(y, X)\right\} \tag{9}$$

The ASD is defined as:

$$ASD(X, Y) = \frac{1}{|X| + |Y|}\left(\sum_{x \in X} d(x, Y) + \sum_{y \in Y} d(y, X)\right) \tag{10}$$

where |X| and |Y| represent the number of voxels in the surface X and Y, respectively.

3. RESULTS

3.1 MR images

The proposed method was evaluated on our prostate MR data set, which consists of 12 T2-weighted volumes. Transverse images were used in the experiments. The voxel sizes of the volumes are from 0.625mm to 1mm. The field of view varies from 200×200 mm^2 to 333×500 mm^2.

3.2 Qualitative evaluation results

The performance of the proposed method is evaluated qualitatively by visual comparison with the manually segmented contours. Meanwhile, the demonstration of the supervoxels is showed in Fig. 3.
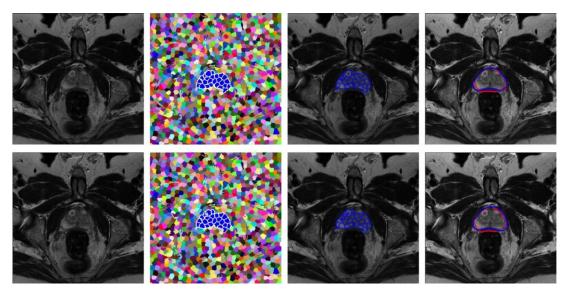
Figure 3. Qualitative evaluation results of the proposed method. The first row is one slice from a typical MR volume, while the second row is the adjacent slice of the same volume. The first column is the original slice. The second column is the supervoxel demonstration. Same color between two slices means the same supervoxel. The blue supervoxels are the segmented prostate obtained from the graph cut. In the third column, the blue boundaries of supervoxels that belong to the prostate are superposed on the original slices to demonstrate the good adherence of the superpvoxel to the boundaries of the prostate. The red curves in the fourth column are the final segmentation obtained by using the 3D level set method. The blue curves are the manual segmented ground truth.
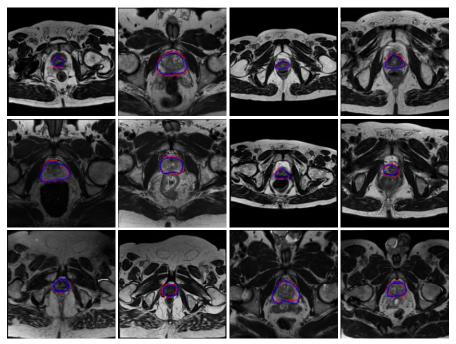

Figure 4. Qualitative results of the proposed method.

The qualitative results from 12 prostate volumes are shown in Fig. 4. Blue curves are manual segmented ground truth by an experienced radiologist, while the red curves are output of the proposed method. Our method has satisfactory results for all the 12 volumes.

3.3 Quantitative evaluation results

The quantitative results are shown in Table 1.

Table 1. Quantitative evaluation of the supervoxel-based prostate segmentation method

	V01	V02	V03	V04	V05	V06	V07	V08	V09	V10	V11	V12	Avg.	Std.
DSC(%)	87.4	89.4	80.3	85.4	89.6	91.0	86.7	87.8	88.6	81.2	88.2	87.1	86.9	3.2
RVD(%)	-8.5	-10.7	32.3	-18.0	-5.7	-9.6	13.0	-9.0	-7.4	-7.8	-5.5	10.7	-2.2	13.9
HD(mm)	6.1	6.1	7.5	6.7	9.5	5.2	8.3	6.4	7.7	8.8	6.2	8.0	7.2	1.3
ASD(mm)	1.4	1.4	1.8	1.5	1.5	1.2	1.4	1.3	1.3	1.9	1.5	1.8	1.5	0.2

Our proposed method yields a mean DSC of 86.9%±3.2%, the RVD of -2.2%±13.9%, the HD of 7.2mm±1.3mm, and ASD of 1.5mm±0.2mm, which are satisfactory in our application.

4. CONCLUSIONS

We proposed a supervoxel-based method to segment the prostate from 3D MR images. The experiments on our MRI data set showed that this method could extract the prostate surface accurately. To the best of our knowledge, this is the first study to use supervoxel for the segmentation of prostate MR images. It reduces the computational and memory cost significantly. Meanwhile, the proposed method makes the graph cuts algorithm to be competent for handling big 3D medical data. The segmentation method can be applied to various applications in prostate imaging.

ACKNOWLEDGMENT

REFERENCES

[1] Siegel, R., Ma, J., Zou, Z., and Jemal, A., "Cancer statistics, 2014," CA: a cancer journal for clinicians, 64(1), 9-29 (2014).

[2] Toth, R., Tiwari, P., Rosen, M., Reed, G., Kurhanewicz, J., Kalyanpur, A., Pungavkar, S., and Madabhushi, A., "A magnetic resonance spectroscopy driven initialization scheme for active shape model based prostate segmentation," Med Image Anal, 15(2), 214-25 (2011).

[3] Wu Qiu, J. Y., Eranga Ukwatta, Yue Sun, Martin Rajchl, and Aaron Fenster, "Prostate Segmentation: An Efficient Convex Optimization Approach With Axial Symmetry Using 3-D TRUS and MR Images," IEEE Transactions on Medical Imaging, 33(4), 947-960 (2014).

[4] Fei, B., Duerk, J. L., Boll, D. T., Lewin, J. S., and Wilson, D. L., "Slice-to-volume registration and its potential application to interventional MRI-guided radio-frequency thermal ablation of prostate cancer," IEEE Trans Med Imaging, 22(4), 515-525 (2003).

[5] Fei, B., Lee, Z., Boll, D. T., Duerk, J. L., Lewin, J. S., and Wilson, D. L., "Image registration and fusion for interventional MRI guided thermal ablation of the prostate cancer." MICCAI, 364-372 (2003).

[6] Litjens, G., Debats, O., Barentsz, J., Karssemeijer, N., and Huisman, H., "Computer-aided detection of prostate cancer in MRI," IEEE transactions on medical imaging, 33(5), 1083-1092 (2014).

[7] Johnson, L. M., Turkbey, B., Figg, W. D., and Choyke, P. L., "Multiparametric MRI in prostate cancer management," Nature Reviews Clinical Oncology, 11(6), 346-353 (2014).

[8] Qiu, W., Yuan, J., Ukwatta, E., Sun, Y., Rajchl, M., and Fenster, A., "Dual optimization based prostate zonal segmentation in 3D MR images," Medical image analysis, 18(4), 660-673 (2014).

[9] Toth, R., and Madabhushi, A., "Multifeature Landmark-Free Active Appearance Models: Application to Prostate MRI Segmentation," IEEE Transactions on Medical Imaging, 31(8), 1638-1650 (2012).

[10] Litjens, G., Toth, R., van de Ven, W., Hoeks, C., Kerkstra, S., van Ginneken, B., Vincent, G., Guillard, G., Birbeck, N., Zhang, J., Strand, R., Malmberg, F., Ou, Y., Davatzikos, C., Kirschner, M., Jung, F., Yuan, J., Qiu, W., Gao, Q., Edwards, P. E., Maan, B., van der Heijden, F., Ghose, S., Mitra, J., Dowling, J., Barratt, D., Huisman, H., and Madabhushi, A., "Evaluation of prostate segmentation algorithms for MRI: The PROMISE12 challenge," Med Image Anal, 18(2), 359-73 (2014).

[11] Guo, Y., Gao, Y., Shao, Y., Price, T., Oto, A., and Shen, D., "Deformable segmentation of 3D MR prostate images via distributed discriminative dictionary and ensemble learning," Medical physics, 41(7), 072303 (2014).

[12] Egger, J., "PCG-Cut: Graph Driven Segmentation of the Prostate Central Gland," Plos One, 8(10), 6 (2013).

[13] Ou, Y., Doshi, J., Erus, G., and Davatzikos, C., "Multi-atlas segmentation of the prostate: A zooming process with robust registration and atlas selection," Medical Image Computing and Computer Assisted Intervention (MICCAI) Grand Challenge: Prostate MR Image Segmentation, 7, 1-7 (2012).

[14] Mahapatra, D., and Buhmann, J. M., "Prostate MRI segmentation using learned semantic knowledge and graph cuts," Biomedical Engineering, IEEE Transactions on 61(3), 756-764 (2014).

[15] Chan, T. F., and Vese, L. A., "Active contours without edges," IEEE transactions on Image processing, 10(2), 266-277 (2001).

[16] Zhang, Y., Matuszewski, B. J., Shark, L., and Moore, C. J., "Medical image segmentation using new hybrid level-set method." 71-76 (2008).

[17] Achanta, R., Shaji, A., Smith, K., Lucchi, A., Fua, P., and Susstrunk, S., "SLIC superpixels compared to state-of-the-art superpixel methods," IEEE Transactions on Pattern Analysis and Machine Intelligence, 34(11), 2274-2282 (2012).

[18] Boykov, Y., Veksler, O., and Zabih, R., "Fast approximate energy minimization via graph cuts," IEEE Transactions on Pattern Analysis and Machine Intelligence, 23(11), 1222-1239 (2001).

[19] Garnier, C., Bellanger, J. J., Wu, K., Shu, H. Z., Costet, N., Mathieu, R., de Crevoisier, R., and Coatrieux, J. L., "Prostate Segmentation in HIFU Therapy," IEEE Transactions on Medical Imaging, 30(3), 792-803 (2011).